THE JOURNAL OF PHYSICAL CHEMISTRY C

Article

pubs.acs.org/JPCC

Effect of Correlation and Dielectric Confinement on $1S^{(e)}_{1/2}nS^{(h)}_{3/2}$ Excitons in CdTe/CdSe and CdSe/CdTe Type-II Quantum Dots

Edward J. Tyrrell and Stanko Tomić*

Joule Physics Laboratory, University of Salford, Manchester M5 4WT, United Kingdom

ABSTRACT: We calculate correlated exciton states in type-II core/shell quantum dots (QDs) using a configuration interaction method combined with the **k·p** theory. We map the $1S^{(e)}_{1/2}1S^{(h)}_{3/2}$ and $1S^{(e)}_{1/2}2S^{(h)}_{3/2}$ exciton correlation energy relative to the strong confinement approximation as a function of core radius, shell thickness, and dielectric confinement. The type-II confinement potentials enhance the effect of dielectric confinement which can significantly affect the wave functions and exciton energies in such heterostructures. Dielectric confinement mainly increases the correlation energy for QDs in which the corresponding single-particle hole states are delocalized. We also find that correlation leads to large changes in the optical dipole matrix element, particularly for the lowest CdSe/CdTe QD exciton, in the presence of dielectric confinement. We conclude that dielectric confinement affected the exciton properties in CdSe/CdTe QDs more than in CdTe/CdSe QDs due to the band alignment which encourages holes to localize in the shell.

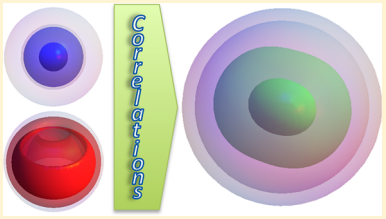

I. INTRODUCTION

Semiconductor nanocrystals or quantum dots (QDs) are the subject of intensive research, due to a number of novel properties which make them attractive for both fundamental studies and technological applications.[1−6] QDs are of particular interest for solar cell applications due to their ability to increase efficiency via the generation of multiexcitons from a single photon.[7−9] QDs can be synthesized with a high degree of control using colloidal chemistry.[10,11] Much research effort has been directed toward studying QDs grown from more than one semiconductor, e.g., core/shell heterostructures.[12−14] Such core/shell nanostructures provide a means to control the optical properties by tuning the electron−hole wave function overlap which is affected by the alignment of the conduction band (CB) and valence band (VB) edges, as well as the QD shape and size. In contrast to type-I band alignments, type-II alignments have staggered CB and VB edges so the lowest energy states for electrons and holes lie in different spatial regions, leading to charge separation between the carriers. Type-II core/shell QDs can be classified according to whether the band alignments tend to localize the hole in the core and electron in the shell (h/e QDs, such as CdTe/CdSe QDs) or the electron in the core and the hole in the shell (e/h QDs, such as CdSe/CdTe QDs).[15] Such staggered band alignments have several useful physical consequences, including longer radiative recombination times for more efficient charge extraction in photovoltaic applications,[16,17] optical gaps that can be made smaller than the bulk values of the constituent materials,[12,18,19] and control of the electron−hole wave function overlap which determines the exchange interaction energy.[20] Charge separation in type-II QDs can also be used to increase the repulsion between like-sign charges in biexciton states,[21,22] leading to the possibility of lasing in the single exciton regime.[6,23,24]

To determine the energetics of many-body states in QDs, both the confinement potential and many-body interactions between the carriers need to be taken into account. Many-body interactions can be classified as Coulomb (charge) and Fermi (spin) correlations. Coulomb correlation arises from the electrostatic interaction of charge carriers in the many-body complex, while spin correlation occurs due to the Fermionic character of the charge carriers (i.e., the Pauli exclusion principle).[25] Correlated many-body states may be calculated with the configuration interaction (CI) method which can be used in the framework of continuum or atomistic descriptions of single-particle states.[26−31]

Colloidal QDs are usually embedded or dispersed in media[32] of lower dielectric constant than the semiconductor itself; this dielectric confinement leads to a modification of the Coulomb interaction which can be described using classical image charge theory. While atomistic calculations[33] showed that dielectric confinement significantly affects the charging energies of QDs, in single-material spherical QDs the similar electron and hole charge distributions lead to a weakened dielectric confinement effect[34] on exciton states which mainly increases the binding energy.[26,35] It is therefore natural to wonder if the optical properties of spherical type-II core/shell QDs can be significantly affected by the dielectric environment.

The effect of dielectric confinement and many-electron correlation means that the single-particle picture is not good enough to faithfully predict exciton energetics or wave functions in colloidal QDs. The proper treatment of charges requires a many-electron description that goes beyond mean-field theories, and the configuration interaction method is one of the most accurate. However, the full configuration method becomes progressively more computationally expensive as the number of states increases. Luckily however the interpretation of physical experiments often requires detailed knowledge of

Received: March 23, 2015
Revised: May 5, 2015
Published: May 5, 2015

ACS Publications © 2015 American Chemical Society

DOI: 10.1021/acs.jpcc.5b02789
J. Phys. Chem. C 2015, 119, 12720−12730

just a few excitons of particular symmetry. To overcome unnecessary computational burden, when analyzing $1S^{(e)}_{1/2}nS^{(h)}_{3/2}$ excitons in core/shell QD structures, we develop a decoupled CI calculation method which only mixes the most important, $ms^{(e)}_{1/2}ns^{(h)}_{3/2}$, single-particle states into the exciton wave function but accurately reproduces the full CI results with greatly reduced computational cost. This allows us to evaluate the effect of correlation on exciton energies and dipole matrix elements for many different core/shell QD geometries, and identify those designs for which correlation effects are greatest.

In this paper we examine the $1S^{(e)}_{1/2}1S^{(h)}_{3/2}$ and $1S^{(e)}_{1/2}2S^{(h)}_{3/2}$ excitons in CdTe/CdSe and CdSe/CdTe QDs using a CI approach to describe the effect of correlation between the electron and hole states. The single-particle states were described using the (2,6)-band **k·p** theory[36] for spherical core/shell QD heterostructures, taking into account correct operator ordering at the heterointerfaces and the complex VB structure.

II. THEORETICAL MODEL

II.A. Single-Particle States. In order to find a set of single-particle (SP) states, we use the (2,6)-band **k·p** Hamiltonian.[36] To illustrate the problem and introduce basic parameters, in Figure 1 we show (a) a schematic of a spherical QD

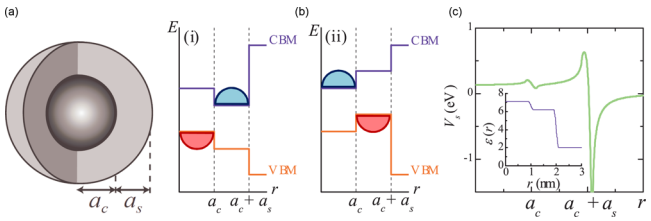

Figure 1. (a) Cutaway view of a spherical core/shell QD; (b) CBM and VBM corresponding to type-II alignment, in (i) an h/e CdTe/CdSe QD and (ii) an e/h CdSe/CdTe QD; (c) typical self-polarization potential for a colloidal CdTe/CdSe QD, with dielectric profile (inset).

characterized by core radius a_c and shell thickness a_s, (b) the staggered alignments of the CB minimum (CBM) and VB maximum (VBM) in type-II h/e CdTe/CdSe and e/h CdSe/CdTe QDs, and (c) a characteristic profile of the self-polarization potential due to the contrast between dielectric constants of the QD and the surrounding medium (colloid). Details of material parameters used can be found in the Appendix.

The electron (hole) SP wave function $\psi^{e(h)}_{j,m,p,n}$ satisfies the Schrödinger equation

$$\hat{H}_{e(h)}\psi^{e(h)}_{j,m,p,n} = E^{e(h)}_{j,p,n}\psi^{e(h)}_{j,m,p,n} \quad (1)$$

where $E^{e(h)}_{j,p,n}$ is the electron (hole) eigenenergy and $\hat{H}_{e(h)}$ is the **k·p** Hamiltonian for electrons (holes). The SP quantum states are denoted using the notation $nl^{(\mu)}_j$, where n is the fundamental quantum number, l = s, p, d, ... represents the lowest value of the orbital angular momentum in the wave function, and $\mu \in$ {e,h} denotes an electron or hole.[37] Due to the macroscopic spherical symmetry of the QD shape and the fact that the material parameters depend on the radial coordinate r only, the states calculated according to the **k·p** theory can be characterized by the total angular momentum j and its z-component $m \equiv j_z$.[36] Furthermore, the parity operator $\hat{P}$ commutes with the Hamiltonian $\hat{H}$ of any system possessing a spherically symmetric confining potential V, so that $\hat{H}$ and $\hat{P}$ share the same set of eigenfunctions. As a result, SP eigenstates in spherical QDs are also characterized by the eigenvalue p of the parity operator; p takes the values 1 and −1 for even and odd states, respectively. In spherical QDs possessing spherically symmetric confinement potentials the parity is conserved. Furthermore, the radial part of the wave function can be classified according to whether it has odd or even parity. In Figures 2 and 3 we show charge densities of n = 1, m = 1/2

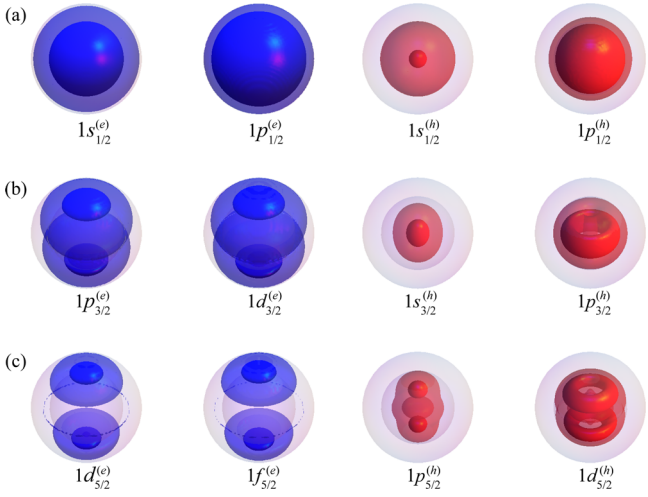

Figure 2. Probability density isosurfaces of SP states in an a_c = 2 nm, a_s = 1 nm CdTe/CdSe QD. Transparent (opaque) surfaces represent 25% (75%) of the maximum value of $|\psi^{e(h)}_{j,m,p,n}|^2$.

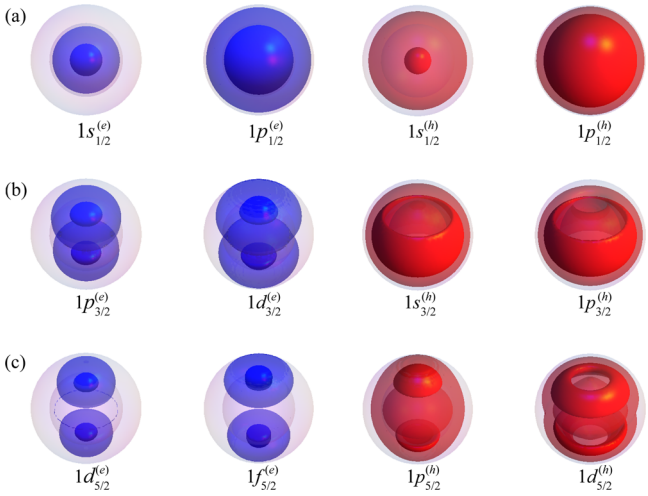

Figure 3. Probability density isosurfaces of SP states in an a_c = 2 nm, a_s = 1 nm CdSe/CdTe QD. Transparent (opaque) surfaces represent 25% (75%) of the maximum value of $|\psi^{e(h)}_{j,m,p,n}|^2$.

electron and hole SP states with (a) j = 1/2, (b) j = 3/2, and (c) j = 5/2 in CdTe/CdSe and CdSe/CdTe QDs, respectively. SP states with j = 1/2 have spherically symmetric charge densities, and all SP states with $m = \pm 1/2$ are symmetric about the z-axis.

II.B. Exciton States. Our SP ket notation $|jmpn\rangle$ is defined in terms of total angular momentum j and parity p, such that $\langle \mathbf{r}_\mu | jmpn\rangle = \psi^{\mu}_{j,m,p,n}(\mathbf{r}_\mu)$. To construct excitonic states, we couple SP states in terms of angular momentum rather than parity, so

DOI: 10.1021/acs.jpcc.5b02789
J. Phys. Chem. C 2015, 119, 12720−12730

we define the new ket notation $|nljm\rangle$ in terms of both total angular momentm j and the lowest value of orbital angular momentum l. In such notation $l = j - p/2$ for electrons and $l = \min(j + p/2, |j - 3p/2|)$ for holes, where $p = +1$ (-1) for even (odd) states regardless of whether electron or hole states are considered.[36]

Exciton Hamiltonian. In the presence of a spatially varying dielectric constant, the exciton Hamiltonian is[26]

$$\hat{H}_X = \hat{H}_e + \hat{H}_h + V_c(\mathbf{r}_e, \mathbf{r}_h) + V_s(\mathbf{r}_e) + V_s(\mathbf{r}_h) \quad (2)$$

where V_c is the interparticle Coulomb potential and V_s is the self-polarization potential due to the interaction of a carrier with its own polarization charge. We note that $V_c = V_d + V_p$, where V_d is the direct interparticle Coulomb potential and V_p is the interface polarization potential.[15,38] Excitonic states are solutions of the Schrödinger equation

$$\hat{H}_X|\Psi_X^{L,L_z}\rangle = E_X|\Psi_X^{L,L_z}\rangle \quad (3)$$

where L is the total exciton angular momentum, L_z is its z-component, and E_X is the exciton eigenenergy. The exciton wave function can be expanded in terms of uncorrelated electron−hole pair (EHP) states as[27]

$$|\Psi_X^{L,L_z}\rangle = \sum_{\beta=\{n_e,l_e,j_e,n_h,l_h,j_h\}} c_\beta|n_e l_e j_e n_h l_h j_h;\, LL_z\rangle \quad (4)$$

where

$$|n_e l_e j_e n_h l_h j_h;\, LL_z\rangle = \sum_{m_e,m_h} C^{L,L_z}_{j_e,m_e;j_h,m_h}|n_e l_e j_e m_e\rangle|n_h l_h j_h m_h\rangle \quad (5)$$

and the $C^{L,L_z}_{j_e,m_e;j_h,m_h}$ are Clebsch−Gordan coefficients. In eq 4 c_β is the expansion coefficient (character) of a particular $ms^{(e)}_{1/2}ns^{(h)}_{3/2}$ ($m, n \in \mathbb{N}$) EHP state labeled by β. Since L and L_z are conserved for correlated exciton states, the Hamiltonian $\hat{H}_x$ can diagonalized separately in different (L,L_z) subspaces.[27]

II.C. Correlation Energy and Momentum. Assuming the form of excitonic wave function in eq 4, the correlation energy of the $1S^{(e)}_{1/2}nS^{(h)}_{3/2}$ ($n \in \mathbb{N}$) excitons can be defined as

$$E_{corr} = E_{X,CI} - E_X \quad (6)$$

where E_X is the exciton energy calculated according to first order perturbation theory (FOPT) inside the strong confinement approximation (SCA) for the exciton wave function.[35,38−40] The probability of excitation from the ground to the exciton state $|\Psi_X^{L,L_z}\rangle$is proportional to the square of the optical dipole matrix element:[41]

$$P_X{}^2 = |\langle 0|\hat{\mathbf{e}}\cdot\hat{\mathbf{p}}_h|\Psi_X^{L,L_z}\rangle|^2 \quad (7)$$

where $\hat{\mathbf{e}}$ is the polarization vector of incident light and $\hat{\mathbf{p}}_h$ is the hole momentum operator. Substituting for $|\Psi_X^{L,L_z}\rangle$ from eq 4 gives

$$P_{X,CI}{}^2 = |\sum_\beta c_\beta\langle 0|\hat{\mathbf{e}}\cdot\hat{\mathbf{p}}_h|n_e l_e j_e n_h l_h j_h;\, LL_z\rangle|^2 \quad (8)$$

where each term in eq 8 must obey the selection rules for electric dipole transitions. Optical dipole matrix elements of the uncorrelated states are calculated as

$$P^2 = |\langle\psi^e_{j,m,p,n}|\hat{\mathbf{e}}\cdot\hat{\mathbf{p}}_h|\psi^h_{j',m',p',n'}\rangle|^2 \quad (9)$$

To assess the effect of correlation on the excitonic optical dipole matrix elements, we define[51]

$$\Delta P_X{}^2 = P_{X,CI}{}^2 - \frac{1}{4}P^2 \quad (10)$$

The *charge density* of the electron (hole) in the correlated exciton is

$$\rho_X^\mu(\mathbf{r}) = \langle\Psi_X^{L,L_z}|\delta(\mathbf{r} - \mathbf{r}_\mu)|\Psi_X^{L,L_z}\rangle \quad (11)$$

However, since $s^{(e)}_{1/2}$ states are spherically symmetric and $s^{(h)}_{3/2}$ states are often approximately spheroidal (see Figures 2 and 3), it is more informative to examine the radial probability density (RPD). The electron RPD is

$$\mathrm{RPD}^e(r) = \frac{1}{4}\sum_{\beta,\beta'} c^*_{\beta'}c_\beta\delta_{n'_h,n_h}[R^{e;1/2,1,n'}_{1/2,0}(r)]^*R^{e;1/2,1,n}_{1/2,0}(r)r^2 \quad (12)$$

Similarly we define a hole RPD as

$$\begin{aligned}\mathrm{RPD}^h(r) = \frac{1}{4}\sum_{\beta',\beta} c^*_{\beta'}c_\beta\delta_{n'_e,n_e}\{&[R^{h;3/2,1,n'}_{3/2,2}(r)]^*R^{h;3/2,1,n}_{3/2,2}(r)\\ &+ [R^{h;3/2,1,n'}_{3/2,0}(r)]^*R^{h;3/2,1,n}_{3/2,0}(r)\\ &+ [R^{h;3/2,1,n'}_{1/2,2}(r)]^*R^{h;3/2,1,n}_{1/2,2}(r)\}r^2\end{aligned} \quad (13)$$

where $R^{\mu;j,p,n}_{l,J}$ is the radial part of the electron (hole) wave function[26,36] and J is the total Bloch function angular momentum. The corresponding SP charge densities are denoted as ρ^μ_{SP}. We also define the probability $p_{c(s)}$ of the SP hole being in the core (shell) region as

$$p_c = \int_0^{a_c}\rho^h_{SP}(r)\,dr, \qquad p_s = \int_{a_c}^{a_c+a_s}\rho^h_{SP}(r)\,dr \quad (14)$$

II.D. Effect of Dielectric Confinement. For colloidal QDs the dielectric constant ε of the QD material is typically much larger than that of the surrounding medium. This dielectric contrast means that any free charge in the QD induces polarization charge in the QD and its surroundings. The overall effect of the induced charge on a source charge is described by the self-polarization potential $V_s(r)$ which shouldn't be ignored, Figure 1c. In colloidal core/shell QDs the self-polarization potential is characterized by a small peak and well near the core/shell interface due to the small dielectric mismatch between the core and shell materials. However, a much larger peak just inside $r = a_c + a_s$ and a deep well slightly outside the QD are due to the far greater dielectric mismatch of the shell and matrix material.

In order to assess the effect of dielectric confinement on the excitonic structure of CdTe/CdSe and CdSe/CdTe core/shell QDs, we performed CI calculations for two different situations: assuming a uniform dielectric constant ε = constant = 6.65 (i.e., the mean of the CdTe and CdSe constants so that dielectric confinement by the surrounding medium and dielectric mismatch of the core and shell were neglected) and using a realistic profile $\varepsilon = \varepsilon(r)$ with the individual dielectric constants for the core, shell, and external medium. In the former case the Coulomb interaction V_c in eq 2 reduces to the direct interparticle term V_d only, allowing us to separate the effects of the interparticle Coulomb attraction and dielectric confinement.

III. RESULTS AND DISCUSSION

III.A. Convergence Considerations. For a general exciton state $|\Psi_X^{L,L_z}\rangle$ there are many combinations of SP states that

DOI: 10.1021/acs.jpcc.5b02789
J. Phys. Chem. C 2015, 119, 12720−12730

should be summed over in eq 5; this number can be reduced by considering the states that can be coupled for specific cases. Angular momentum coupling conditions mean that for optically active $L = 1$ states $|j_e - j_h| \leq 1$ and assuming $L_z = 1$ means $m_e + m_h = 1$. If incident light is polarized parallel to the z-axis, only EHPs with $m_e = m_h = 1/2$ are excited. These assumptions still leave a large number of possible basis states to calculate matrix elements for, since $|n_e l_e j_e n_h l_h j_h; LL_z\rangle$ in eq 5 must be expanded over different ordinal quantum numbers n_μ and angular momenta l_μ. To investigate the relative importance of different SP states, we calculate E_X as a function of the number of states in the EHP basis. We include hole states up to $j = 15/2$ and all confined electron states in a *full configuration interaction* (FCI) scheme.

Figure 4 shows the convergence of the exciton energy E_X^{FCI} calculated in the FCI scheme for the $1S_{1/2}^{(e)}1S_{3/2}^{(h)}$ exciton against

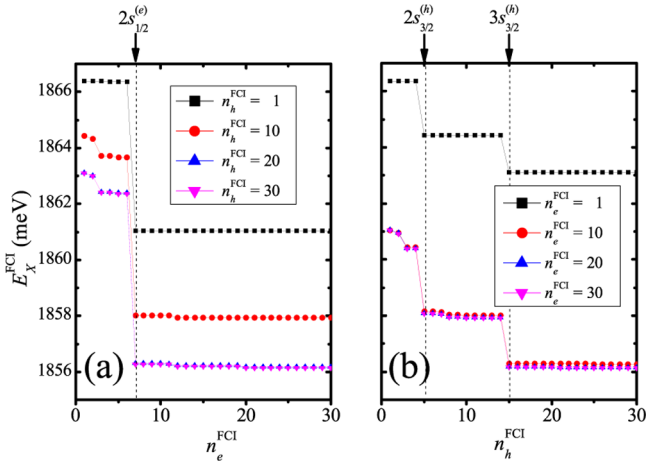

Figure 4. Convergence of E_X^{FCI} as a function of (a) n_e^{FCI} and (b) n_h^{FCI} for $a_c = 2$ nm, $a_s = 0.5$ nm CdTe/CdSe QD.

(a) the number of electron states n_e^{FCI} and (b) the number of hole states n_h^{FCI} in the basis. We see that E_X^{FCI} changes in a stepwise fashion with the addition of extra states to the basis—falling from its FOPT value of 1866.38 meV to 1856.13 meV when $n_e^{FCI} = n_h^{FCI} = 30$. For $n_h = 20$ the energy E_X^{FCI} changes by 5−6 meV at $n_e^{FCI} = 7$, while when $n_e = 20$ is fixed the energy E_X^{FCI} changes by ∼2 meV at $n_h^{FCI} = 5$ and by an additional ∼1 meV at $n_h^{FCI} = 15$. We have identified that the seventh electron state in the FCI basis is the $2s_{1/2}^{(e)}$ state, while the fifth and fifteenth hole states are the $2s_{3/2}^{(h)}$ and $3s_{3/2}^{(h)}$ states respectively; the positions of these SP states are indicated by arrows at the top of Figure 4. These results suggest that the $1S_{1/2}^{(e)}nS_{3/2}^{(h)}$ ($n \in \mathbb{N}$) excitons are mainly composed of $ms_{1/2}^{(e)}ns_{3/2}^{(h)}$ ($m, n \in \mathbb{N}$) EHPs. Therefore, we developed a *decoupled configuration interaction* (DCI) scheme in which the EHP basis consists solely of $ms_{1/2}^{(e)}ns_{3/2}^{(h)}$ ($m, n \in \mathbb{N}$) pair states. Then the calculation represented in Figure 4 is fully reproduced by the DCI scheme which includes only the first two $s_{1/2}^{(e)}$ states and first three $s_{3/2}^{(h)}$ states. The FCI calculation gave $E_X^{FCI} = 1856.13$ and 2055.88 meV for the $1S_{1/2}^{(e)}1S_{3/2}^{(h)}$ and $1S_{1/2}^{(e)}2S_{3/2}^{(h)}$ excitons, respectively, while the DCI calculation gave $E_X^{DCI} = 1857.00$ and 2057.29 meV for the same states (equivalent to relative errors of -1.4×10^{-2} and -5.1×10^{-2}%, respectively).[52] Due to the greatly reduced computational load all relevant results are easily converged within this framework.

III.B. Comparison with Experiment. The $1S_{1/2}^{(e)}nS_{3/2}^{(h)}$ (n = 1, 2) states are the two lowest energy excitons observed in the absorption spectra of colloidal CdTe/CdSe nanocrystals (NCs),[21,39,42] making them the most important for understanding the near band-edge absorption characteristics of such nanoparticles. Figure 5 shows the $1S_{1/2}^{(e)}1S_{3/2}^{(h)}$ and $1S_{1/2}^{(e)}2S_{3/2}^{(h)}$

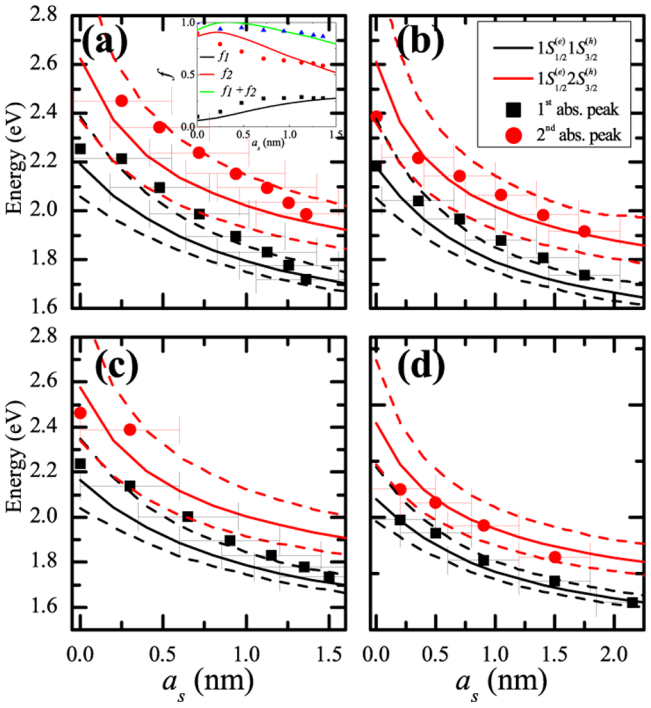

Figure 5. Energies of the $1S_{1/2}^{(e)}nS_{3/2}^{(h)}$ (n = 1, 2) excitons calculated in the DCI scheme (lines) for CdTe/CdSe QDs with (a) $a_c = 1.7$ nm, (b) $a_c = 1.72$ nm, (c) $a_c = 1.75$ nm, and (d) $a_c = 1.95$ nm. Experimental data taken from refs 42, 43, 44, and 21 are shown as filled symbols. Error bars represent an uncertainty of 1 ML (≈±0.3 nm) in the shell thickness. Dashed lines show upper and lower limits on the exciton energies resulting from an uncertainty of 1 ML in the nominal core radii.

exciton energies (solid lines) calculated in the DCI scheme as a function of shell thickness for CdTe/CdSe QDs with (a) a_c = 1.7 nm, (b) a_c = 1.72 nm, (c) a_c = 1.75 nm, and (d) a_c = 1.95 nm. Dashed lines show upper and lower limits on the exciton energies resulting from an uncertainty of 1 monolayer (ML) in the displayed core radii (∼±0.3 nm). Filled circles in Figure 5 show exciton energies taken from the first and second absorption peak positions in absorption spectra measured by (a) Gong et al.,[42] (b) Ma et al.,[43] (c) Cai et al.,[44] and (d) Oron et al.[21] We see good quantitative agreement between the calculated exciton energies and the experimental data, with the data lying in the channels defined by an uncertainty of ±1 ML width in the core size. It should be noted that the results of Oron et al.[21] were obtained on zinc-blende NC structures, in addition to those of Cai et al.[44] The papers by Gong et al.[42] and Ma et al.[43] do not explicitly state the crystal structures of the core/shell nanoparticles, although Ma et al.[43] note that their core/shell NCs gave absorption and photoluminescence spectra very similar to those of Cai and co-workers.[44] Our calculations accurately reproduce the 0.25 eV energy separation between the $1S_{1/2}^{(e)}1S_{3/2}^{(h)}$ and $1S_{1/2}^{(e)}2S_{3/2}^{(h)}$ excitons that is nearly independent of shell thickness.[42] This constant energy separation is characteristic of changing electron confinement

DOI: 10.1021/acs.jpcc.5b02789
J. Phys. Chem. C 2015, 119, 12720−12730

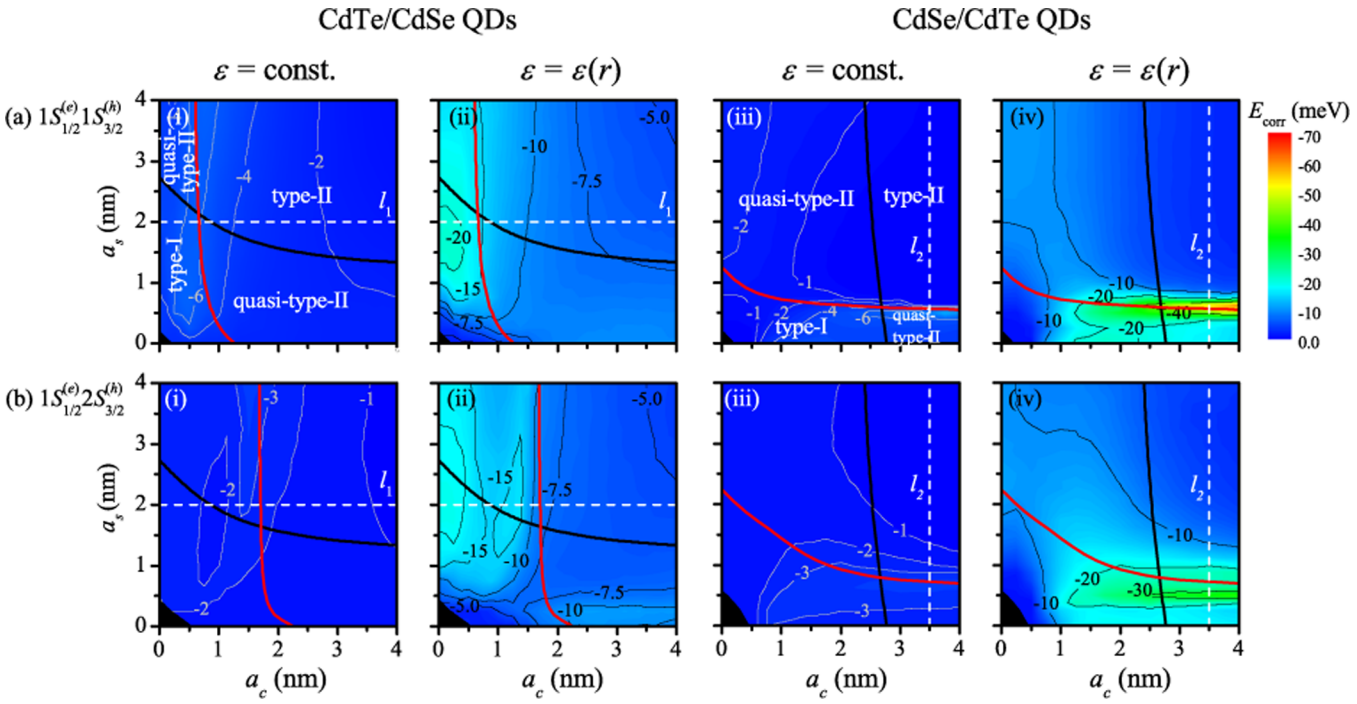

Figure 6. Correlation energy, E_{corr}, of the (a) $1S^{(e)}_{1/2}1S^{(h)}_{3/2}$ and (b) $1S^{(e)}_{1/2}2S^{(h)}_{3/2}$ excitons in CdTe/CdSe and CdSe/CdTe QDs. (i) and (iii) correspond to ε = const., while (ii) and (iv) correspond to $\varepsilon = \varepsilon(r)$, respectively. Electron (hole) LBs are shown as black (red) lines.

but approximately constant hole confinement in the h/e heterostructure. We also find good agreement between the oscillator strength obtained by Gong et al.[42] from the absorption spectra and our calculations. Calculating the oscillator strength f_n of the $1S^{(e)}_{1/2}nS^{(h)}_{3/2}$ (n = 1, 2) excitons as $f_n = 2P_{X,DCI}{}^2/m_0E_{X,DCI}$, we find that $f_1 + f_2 \sim$ constant (inset Figure 5), confirming the validity of relevant excitonic wave functions too.

III.C. Correlation Energies. Figure 6 shows E_{corr} values for the $1S^{(e)}_{1/2}1S^{(h)}_{3/2}$ and $1S^{(e)}_{1/2}2S^{(h)}_{3/2}$ excitons in CdTe/CdSe and CdSe/CdTe QDs. Black and red lines represent the localization boundaries (LBs) for the electron and hole, respectively.[15] In the CdTe/CdSe QD the electron is classified as shell-localized if its energy lies below the CBM of the core material, while the hole is core-localized if its energy lies above the VBM of the shell material. Similar criteria apply for the CdSe/CdTe QD. The type-I regime is defined by both carriers being delocalized over the entire QD, with their energies mainly determined by the "global confinement" provided by the potential well of radius $a_c + a_s$. The type-II regime corresponds to the carriers being localized in different regions of the QD (i.e., the hole in the core and the electron in the shell for the h/e QD and the reverse for the e/h QD), so the SP energies are mainly determined by the dimensions of the relevant region. The quasi-type-II regime corresponds to partial charge separation; in the h/e QD this corresponds to a delocalized hole and shell-localized electron or a core-localized hole and delocalized electron in the e/h QD.

Areas of significant magnitude correlation energy in Figure 6 always roughly coincide with those associated with large optical dipole matrix elements for the corresponding uncorrelated EHPs.[39] In those regions the electron−hole correlation is enhanced as the SP wave function overlap is high and the interparticle Coulomb matrix elements are increased in magnitude. In the type-II regimes $|E_{corr}|$ is mainly small since the spatial separation of the electron and hole (induced by the type-II band alignment) overrides Coulomb attraction. In those regions the exciton wave function is closer to being described by the SCA. Although areas of high $|E_{corr}|$ partly overlap with the type-II regions, the trend is for $E_{corr} \to 0$ in the type-II localization limit. The highest $|E_{corr}|$ values in Figure 6 are a consequence of dielectric confinement affecting the correlated hole density [see Figure 6a(iv),b(iv)], reflected by the fact that they mainly occur in regions where the corresponding SP hole is delocalized. For example, in CdTe/CdSe QDs dielectric mismatch increases $|E_{corr}|$ for the $1S^{(e)}_{1/2}nS^{(h)}_{3/2}$ (n = 1, 2) excitons in structures in which the corresponding $nS^{(h)}_{3/2}$ states are delocalized (or approximately so) over the whole QD. Once strongly core-localized (right of the LB), such SP hole states have little or no overlap with the self-polarization potential near the QD/medium interface. Similarly dielectric mismatch mostly affects E_{corr} for the $1S^{(e)}_{1/2}nS^{(h)}_{3/2}$ (n = 1, 2) excitons in CdSe/CdTe QDs which lie below or near the hole LB (corresponding to delocalized SP holes). Figure 6a(iv),b(iv) also shows that E_{corr} has a distinct minimum as a function of a_s. This minimum is due to the fact that an increase in a_s causes the hole density to shift into the shell where it starts to be affected by the self-polarization potential at the QD/medium interface. However, as a_s increases further, the hole localizes completely in the shell so that spatial confinement by the VBM overrides the repulsive effect of the self-polarization potential causing $E_{corr} \to 0$; see section III.D.2 for further explanations.

For the $1S^{(e)}_{1/2}1S^{(h)}_{3/2}$ exciton the area of nonzero E_{corr} in the lower right quasi-type-II regime of the CdTe/CdSe QD in Figure 6a(ii), is equivalent to the area in the upper left quasi-type-II regime of the CdSe/CdTe QD in Figure 6a(iv). Similarly, the region of large $|E_{corr}|$ for the $1S^{(e)}_{1/2}2S^{(h)}_{3/2}$ exciton at $a_c \gtrsim 2$ nm, $a_s \lesssim 0.5$ nm in Figure 6b(ii) is analogous to the area at $a_c \lesssim 2.5$ nm, $a_s \gtrsim 1.5$ nm in Figure 6b(iv).

Overall we find that dielectric confinement affects the correlated hole density more than the correlated electron density for two reasons. First, the larger effective mass and

DOI: 10.1021/acs.jpcc.5b02789
J. Phys. Chem. C 2015, 119, 12720−12730

deeper potential well experienced by SP hole states compared to electron states allow the former to localize more fully in the shell, closer to the peak in $V_s(r)$ at $r \simeq a_c + a_s$. Second, the smaller energy spacing between the hole SP basis states (i.e., the larger density of hole states) compared to electron SP basis states means that the resulting correlated hole density has more "degrees of freedom" to adjust to the effects of dielectric confinement.

III.D. Correlated Exciton States. *III.D.1. CdTe/CdSe QD: Effect of Electron Shell Localization.* In Figure 7 we present E_{corr} values for the $1S^{(e)}_{1/2}1S^{(h)}_{3/2}$ and $1S^{(e)}_{1/2}2S^{(h)}_{3/2}$ excitons as a function of core radius for fixed shell a_s = 2 nm CdTe/CdSe QDs (line l_1 in Figure 6).

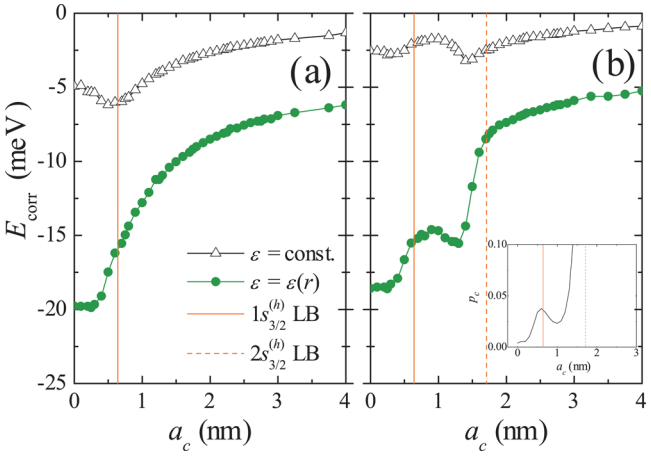

Figure 7. E_{corr} of (a) $1S^{(e)}_{1/2}1S^{(h)}_{3/2}$ and (b) $1S^{(e)}_{1/2}2S^{(h)}_{3/2}$ excitons in a_s = 2 nm CdTe/CdSe QDs along the line l_1 in Figure 6. Cases of ε = const. and $\varepsilon = \varepsilon(r)$ are represented by open and solid symbols, respectively. The inset shows p_c for the $2s^{(h)}_{3/2}$ SP state.

We see that in the presence of dielectric confinement $|E_{corr}| \lesssim$ 20 meV for both excitons and that E_{corr} exhibits at least one minimum as a function of a_c in the ε = const. and $\varepsilon = \varepsilon(r)$ cases. $|E_{corr}|$ is up to 4 times greater in the presence of dielectric confinement ($\varepsilon = \varepsilon(r)$) compared to the ε = const. case. This result highlights the importance of a proper treatment of the dielectric environment in such nanostructures. The minimum in E_{corr} for the $1S^{(e)}_{1/2}1S^{(h)}_{3/2}$ exciton, Figure 7a, is a consequence of two competing effects: proximity of the self-polarization potential peak which tends to reduce the electron−hole separation and the effect of the type-II confinement profile which tends to separate the carriers as a_c increases. However, for the $1S^{(e)}_{1/2}2S^{(h)}_{3/2}$ exciton E_{corr} is not a monotonic function of a_c for either $\varepsilon = \varepsilon(r)$ or ε = const. Insight into the QD size dependence of E_{corr} can be gained by considering the amount of probability density in the core and shell associated with the dominant SP hole state that the correlated exciton originates from. The inset in Figure 7b shows the amount of $2s^{(h)}_{3/2}$ hole probability density in the core as a function of a_c, demonstrating a similar qualitative a_c dependence to E_{corr} in the dielectric mismatch case. We expect an increase in p_c to cause a decrease in $|E_{corr}|$ since a greater amount of hole density in the core leads to less overlap with electron density in the shell and less correlation.

$1S^{(e)}_{1/2}1S^{(h)}_{3/2}$ Exciton. Figure 8 shows the RPDs of the correlated $1S^{(e)}_{1/2}1S^{(h)}_{3/2}$ exciton (solid lines) compared to the $1s^{(e)}_{1/2}1s^{(h)}_{3/2}$ EHP (dotted lines) as a function of a_c when (i) ε = const. and (ii) $\varepsilon = \varepsilon(r)$. The shifts due to the direct interparticle

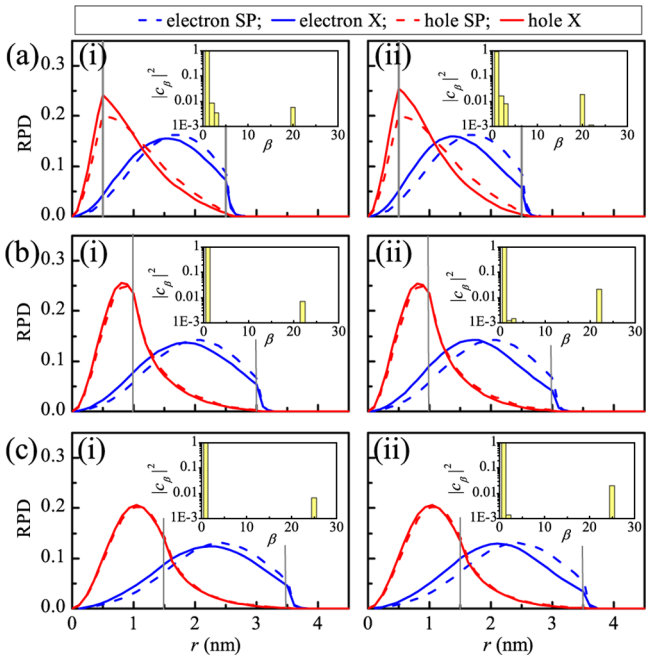

Figure 8. Solid (dashed) lines represent RPDs of the $1S^{(e)}_{1/2}1S^{(h)}_{3/2}$ exciton ($1s^{(e)}_{1/2}1s^{(h)}_{3/2}$ EHP) of CdTe/CdSe QDs with a_s = 2 nm and (a) a_c = 0.5 and (b) a_c = 1.5 nm for (i) ε = const. and (ii) $\varepsilon = \varepsilon(r)$. Vertical lines denote the boundaries between the core, shell, and external medium. Insets are bar charts of $|c_\beta|^2$ characters.

Coulomb interaction are relatively small when ε = const. and both carriers move slightly toward the core. By increasing a_c to ∼1 nm and beyond, the hole mainly localizes in the core so that $\rho^h_X \simeq \rho^h_{SP}$ and the SCA regime is reached, where the spatial confinement outweighs the effect of correlations.

When $\varepsilon = \varepsilon(r)$, the increased values of $|E_{corr}|$ are associated with a shift of RPD away from the QD surface due to repulsion by the large peak in the self-polarization potential near $r = a_c + a_s$. The correlated electron is affected more since the electron SP states tend to localize in the shell. The exciton wave function gains $2s^{(e)}_{1/2}1s^{(h)}_{3/2}$ character corresponding to the β = 20 and β = 25 EHP for the a_c = 0.5 and 1.5 nm QDs, respectively. The hole is only slightly affected by the self-polarization potential near the QD surface when there is a significant amount of hole charge density in the shell, as in the case of small a_c.

$1S^{(e)}_{1/2}2S^{(h)}_{3/2}$ Exciton. In the absence of dielectric confinement $|E_{corr}|$ is always small (≲3 meV) because the exciton state is very close to the $1s^{(e)}_{1/2}2s^{(h)}_{3/2}$ (β = 2) EHP state and $|c_2|^2 \simeq 1$. When $\varepsilon = \varepsilon(r)$ the trend is very similar to the $1S^{(e)}_{1/2}1S^{(h)}_{3/2}$ exciton, except different EHP characters are involved. For example, in the a_c = 1 nm QD the correlated exciton wave function is mainly composed of the β = 3, 4, and 23 ($1s^{(e)}_{1/2}3s^{(h)}_{3/2}$, $1s^{(e)}_{1/2}4s^{(h)}_{3/2}$, $2s^{(e)}_{1/2}2s^{(h)}_{3/2}$) EHPs, while in the a_c = 1.5 nm QD, the β = 3 and 26 ($1s^{(e)}_{1/2}3s^{(h)}_{3/2}$, $2s^{(e)}_{1/2}2s^{(h)}_{3/2}$) EHPs are dominant. Again, when the hole localizes in the core, only the electron is significantly affected by dielectric mismatch.

III.D.2. CdSe/CdTe QD: Effect of Hole Shell Localization. In Figure 9 we present E_{corr} values for the $1S^{(e)}_{1/2}1S^{(h)}_{3/2}$ and $1S^{(e)}_{1/2}2S^{(h)}_{3/2}$ excitons as a function of shell thickness for an a_c = 3.5 nm fixed core in CdSe/CdTe QDs (line l_2 in Figure 6). We observe the largest size correlation energy of the considered excitons for the $1S^{(e)}_{1/2}1S^{(h)}_{3/2}$ state in CdSe/CdTe QDs when $\varepsilon = \varepsilon(r)$, with E_{corr} reaching −62 meV for an a_c = 3.5 nm, a_s = 0.6

DOI: 10.1021/acs.jpcc.5b02789
J. Phys. Chem. C 2015, 119, 12720−12730

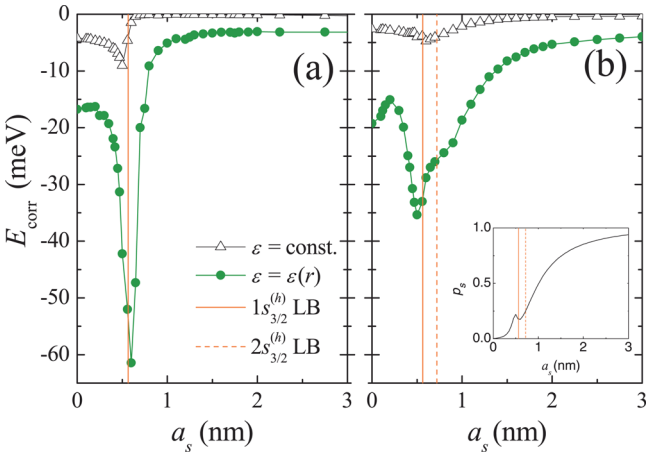

Figure 9. E_{corr} of (a) $1S^{(e)}_{1/2}1S^{(h)}_{3/2}$ and (b) $1S^{(e)}_{1/2}2S^{(h)}_{3/2}$ excitons in a_c = 3.5 nm CdSe/CdTe QDs along the line l_2 in Figure 6. Cases of ε = const. and $\varepsilon = \varepsilon(r)$ are represented by open and solid symbols, respectively. The inset shows p_s for the $2s^{(h)}_{3/2}$ SP state.

nm QD, Figure 9a. This value is more than 6 times larger than the corresponding value for the ε = const. case, highlighting the particularly strong effect of the dielectric environment on this exciton. It can be observed from Figure 9 that the effect of dielectric mismatch on E_{corr} is strongest in the vicinity of the $1s^{(h)}_{3/2}$ LB, i.e., once the SP hole becomes delocalized over the QD.

We found the second largest $|E_{corr}|$ value for the CdSe/CdTe QD $1S^{(e)}_{1/2}2S^{(h)}_{3/2}$ exciton, with E_{corr} = −36 meV for an a_s = 0.5 nm QD. Again, this minimum is observed in the vicinity of the $1s^{(h)}_{3/2}$ and $2s^{(h)}_{3/2}$ LBs where those two hole states become delocalized over the QD. The maximum value of $|E_{corr}|$ is almost 9 times larger in the presence of dielectric confinement compared to its absence. We note that the curves for E_{corr} and the amount of hole RPD in the shell p_s have qualitatively similar a_s dependences to the right of the $1s^{(h)}_{3/2}$ LB; see the inset in Figure 9b. An increase in p_s is associated with a decrease in the amount of hole RPD that overlaps with the core-localized electron leading to a decrease of electron−hole correlation and causing $E_{corr} \to 0$.

$1S^{(e)}_{1/2}1S^{(h)}_{3/2}$ Exciton. In the case of a core-only CdSe QD and no dielectric confinement, correlation causes both carriers to move toward the center of the QD compared to their SP counterparts, Figure 10a(i). This is purely a result of the direct interparticle Coulomb interaction, giving correlation energies of approximately −5 meV. Introduction of the self-polarization potential, i.e., $\varepsilon = \varepsilon(r)$, further enhances this move of RPDs of both carriers away from the QD surface in the core-only CdSe QD, Figure 10a(ii). This effect increases localization of both carriers near the center of QD, increasing their overlap and giving correlation energies E_{corr} = −18 meV. For the $1S^{(e)}_{1/2}1S^{(h)}_{3/2}$ exciton in the CdSe QD, the shift in RPD is mainly due to an increase in $2s^{(e)}_{1/2}1s^{(h)}_{3/2}$ (β = 26) character.

To assess the effect of dielectric confinement on the correlated carriers in the CdSe QD, we consider the expectation value of the 1s electron (hole) radial coordinate, denoted $\langle r_\mu \rangle$. When ε = const. (no self-polarization) we find $\langle r_h \rangle$ = 1.55 nm, compared to $\langle r_h \rangle$ = 1.44 nm when $\varepsilon = \varepsilon(r)$ for the $1s^{(h)}_{3/2}$ state. In contrast, the effect of dielectric confinement moves the $1s^{(e)}_{1/2}$ electron from $\langle r_e \rangle$ = 2.01 nm to $\langle r_e \rangle$ = 1.89. Although the SP $1s^{(e)}_{1/2}$ RPD has significantly greater overlap with the repulsive peak in self-polarization potential near the QD surface than the

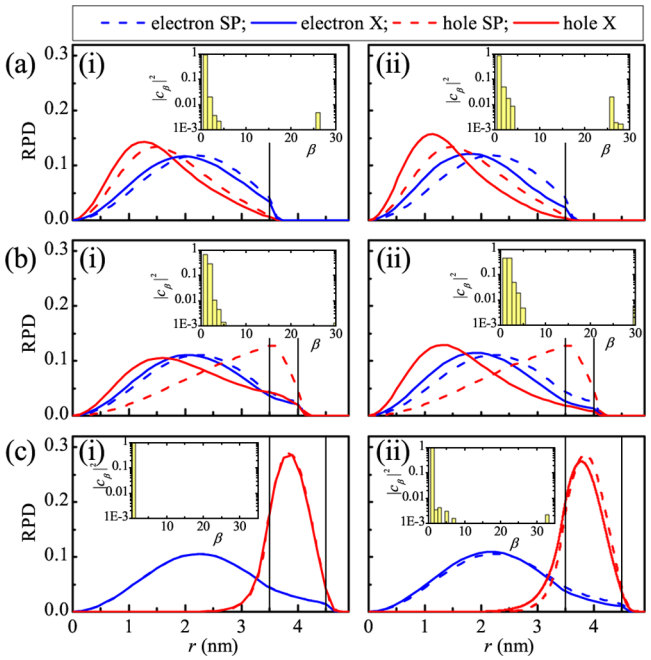

Figure 10. Solid (dashed) lines represent RPDs of the $1S^{(e)}_{1/2}1S^{(h)}_{3/2}$ exciton ($1s^{(e)}_{1/2}1s^{(h)}_{3/2}$ EHP) of CdSe/CdTe QDs with a_c = 3.5 nm and (a) a_s = 0, (b) a_s = 0.5 nm, and (b) a_s = 1 nm for (i) ε = const. and (ii) $\varepsilon = \varepsilon(r)$. Vertical lines denote the boundaries between the core, shell, and external medium. Insets are bar charts of $|c_\beta|^2$ characters.

SP $1s^{(h)}_{3/2}$ hole RPD, the correlated electron is shifted by dielectric confinement by almost the same distance as the correlated hole. These results reflect the larger sensitivity of the correlated hole wave function to the dielectric environment compared to the electron in the CdSe core-only QD.

In Figure 10b(i) we see that the introduction of a thin CdTe shell allows the uncorrelated hole to start to localize near the QD surface (at $r = a_c + a_s$), dramatically reducing its overlap with the uncorrelated electron. However, when ε = const. the introduction of correlation alone is strong enough to pull the hole back toward the center of the QD, mainly due to the addition of the $1s^{(e)}_{1/2}2s^{(h)}_{3/2}$ (β = 2) EHP to the exciton wave function. We see that the introduction of dielectric confinement again enhances this move of the carriers further away from the QD surface compared to the ε = const. case. The effect of dielectric confinement is particularly strong in this case because $\langle r_h \rangle$ for the $1s^{(h)}_{3/2}$ state is close to the value of QD's outermost radius, $a_c + a_s$.

The close proximity of the hole to QD surface reduces the distance $\xi = \langle r_h^{QD} \rangle - \langle r_h^{image} \rangle$ between the hole in the QD and its mirror image in the colloid, dramatically increasing the Coulombic repulsion between them which scales as $1/\xi$. Such repulsion causes the hole to be pushed back toward the center of the QD, thereby dramatically increasing overlap with the correlated electron wave function. The presence of dielectric confinement means the exciton wave function is an almost equal superposition of the $1s^{(e)}_{1/2}ns^{(h)}_{3/2}$ (n = 1, 2) states, with $|c_1|^2$ = 0.449 and $|c_2|^2$ = 0.458 (inset in Figure 10b(ii)). For comparison, when ε = const. the $1s^{(e)}_{1/2}2s^{(h)}_{3/2}$ character amounts to only $|c_2|^2$ = 0.019. The much stronger configuration mixing in the dielectric confinement case allows E_{corr} to reach −62 meV, compared to −9 meV without dielectric confinement.

Further increase of the CdSe/CdTe QD shell thickness to a_s = 1 nm allows the SP hole to fully localize in the shell while the

DOI: 10.1021/acs.jpcc.5b02789
J. Phys. Chem. C 2015, 119, 12720−12730

SP electron stays in the core, reaching the type-II localization limit. The carriers effectively enter the strong confinement regime in which the Coulomb effects are overridden by the effects of the type-II spatial confinement. In the SCA $\rho_X^{e(h)} \simeq \rho_{SP}^{e(h)}$, and the effect of correlations is lost. Again, E_{corr} is only nonzero when the hole is delocalized; once it localizes in the shell, the effect of VBM confinement overrides the interparticle Coulomb attraction. Dielectric confinement only slightly shifts the hole density toward the core, resisted by the opposing effect of spatial confinement with $E_{corr} \approx -3$ meV for $a_s > 1.5$ nm.

$1S_{1/2}^{(e)}2S_{3/2}^{(h)}$ Exciton. In the absence of dielectric mismatch (ε = const.) the interparticle Coulomb interaction mainly causes the hole to move toward the core while the electron is nearly unaffected, Figure 11a(i)−c(i). Introducing dielectric confinement systematically moves the hole RPD toward the center of the QD, while the electron is again minimally affected, Figure 11a(ii)−c(ii). Dielectric confinement has the most pronounced effect on the a_s = 0.5 nm QD for which the self-polarization potential is able to almost completely repel the hole RPD from the shell to the core region, Figure 11b(ii); this is associated with an increase of $|E_{corr}|$ to 36 meV. The movement of the correlated hole RPD to the center of the QD upon introduction of dielectric confinement is due to the mixing of $1s_{1/2}^{(e)}ns_{3/2}^{(h)}$ (n = 1, 2) EHPs into the exciton wave function. For the a_s = 1 nm QD the competing effects of type-II VBM profile, interparticle Coulomb attraction, and self-polarization potential lead to the correlated hole RPD being delocalized across the whole QD with a local maximum in both the core and shell. When a_s is increased to 1.5 nm and beyond, the SCA regime is reached and the correlated RPDs are very close to those of the uncorrelated states (not shown).

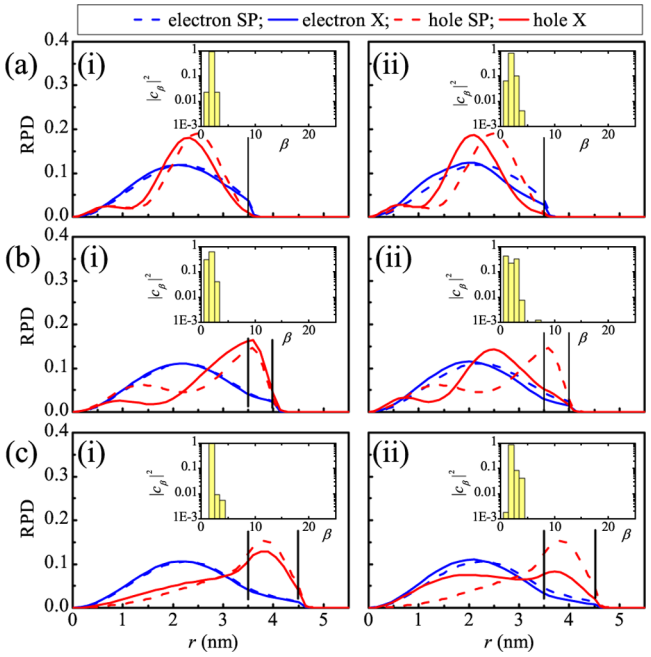

Figure 11. Solid (dashed) lines represent RPDs of the $1S_{1/2}^{(e)}2S_{3/2}^{(h)}$ exciton ($1s_{1/2}^{(e)}2s_{3/2}^{(h)}$ EHP) of CdSe/CdTe QDs with a_c = 3.5 nm and (a) a_s = 0, (b) a_s = 0.5 nm, and (b) a_s = 1 nm for (i) ε = const. and (ii) $\varepsilon = \varepsilon(r)$. Vertical lines denote the boundaries between the core, shell and external medium. Insets are bar charts of $|c_\beta|^2$ characters.

Generally we have observed when the correlated wave functions are in the type-II localization regime the charge that localizes in the QD's shell is affected more by the interparticle Coulomb attraction while the innermost confined charge carrier is barely affected. We explain this behavior from the fact that $s_{1/2}^{(e)}$ electron states are largely spherically symmetric (see Figure 2a) and core-localized $s_{3/2}^{(h)}$ hole states are approximately spheroidal (see Figure 2b). Gauss's law means that hole charge density ρ_X^h at some radius r_h is not affected any more by electron charge density ρ_X^e situated at $r > r_h$.

III.E. Exciton Optical Dipole Matrix Elements. The regions of largest $|\Delta P_X{}^2|$ in Figure 12 closely coincide with the regions of largest $|E_{corr}|$ in Figure 6 since the greater the change in carrier density due to correlation the greater the change in electron−hole wave function overlap. However, the correlation can increase or decrease the dipole matrix element of a particular exciton state relative to the SCA depending on the localization regime of the uncorrelated charge carriers.

Correlation only slightly changes the dipole matrix elements of the $1S_{1/2}^{(e)}1S_{3/2}^{(h)}$ CdTe/CdSe QD exciton, which is consistent with the similarity of the correlated and uncorrelated carrier RPDs in Figure 8. For the CdTe/CdSe QD we see that when ε = const. the $\Delta P_X{}^2 = 0$ contour closely follows the $1s_{3/2}^{(h)}$ LB (see Figure 12a(i)), indicating that the $1s_{3/2}^{(h)}$ hole should be delocalized (or approximately so) for correlation to reduce the dipole matrix element relative to the uncorrelated EHP. Once the hole localizes in the core, $\Delta P_X{}^2$ becomes positive. Similar behavior is seen when $\varepsilon = \varepsilon(r)$, except that $\Delta P_X{}^2$ can be slightly negative for QDs with thin shells, $a_s \lesssim 0.5$ nm.

Figure 12a(iii,iv) shows a similar trend for the CdSe/CdTe QD, with $\Delta P_X{}^2$ only being negative when the $1s_{3/2}^{(h)}$ hole is delocalized; this is particularly noticeable for CdSe/CdTe QDs with $a_c \gtrsim 1.5$ nm when $\varepsilon = \varepsilon(r)$ in Figure 12a(iv). As the shell width increases for a particular core radius $\Delta P_X{}^2$ increases dramatically near the $1s_{3/2}^{(h)}$ LB; this is due to the interparticle Coulomb interaction that prevents the hole wave function localizing in the shell and dramatically increases its overlap with the electron wave function in the core, Figure 10b. This effect is enhanced by dielectric confinement, shown by the larger brighter area in Figure 12a(iv) above the hole LB. The difference $\Delta P_X{}^2$ reaches a maximum value of 0.15 for an a_c = 3.5 nm, a_s = 0.75 nm QD when $\varepsilon = \varepsilon(r)$, compared to a maximum value of 0.042 (for an a_c = 3 nm, a_s = 0.625 nm QD) when ε = const.. These shifts represent an increase by a factor of 7.29 and 1.5 in the dipole matrix element respectively relative to the SCA results found using FOPT. Both regions of positive $\Delta P_X{}^2$ seen in Figure 12a(iii,iv) near the hole LB are mainly due to the mixing of the $1s_{1/2}^{(e)}2s_{3/2}^{(h)}$ EHP which becomes a large component of the exciton wave function.

The effect of correlation in the $1S_{1/2}^{(e)}2S_{3/2}^{(h)}$ exciton leads to reduction of dipole matrix element near the $2s_{3/2}^{(h)}$ LB in both the CdTe/CdSe and CdSe/CdTe QD. This is most clearly seen for the CdSe/CdTe QD in Figure 12b(iii,iv), for which the reduction in the contribution of the $1s_{1/2}^{(e)}2s_{3/2}^{(h)}$ EHP leads to the an area of negative $\Delta P_X{}^2$. These areas roughly coincide with the regions of positive $\Delta P_X{}^2$ in Figure 12a(iii,iv), suggesting a transfer of oscillator strength from the $1S_{1/2}^{(e)}1S_{3/2}^{(h)}$ to $1S_{1/2}^{(e)}2S_{3/2}^{(h)}$ CdSe/CdTe QD exciton.

The $\Delta P_X{}^2$ reaches its maximum value for an a_c = 3.5 nm and a_s = 0.75 nm QD, Figure 13. At this point the radiative recombination time of the $1S_{1/2}^{(e)}1S_{3/2}^{(h)}$ exciton calculated with FOPT (τ_{rad}^{FOPT} = 13.4 ns) is about 1 order of magnitude larger than that calculated with DCI (τ_{rad}^{DCI} = 2.85 ns). This reflects the need for a proper treatment of correlation effects in the design

DOI: 10.1021/acs.jpcc.5b02789
J. Phys. Chem. C 2015, 119, 12720−12730

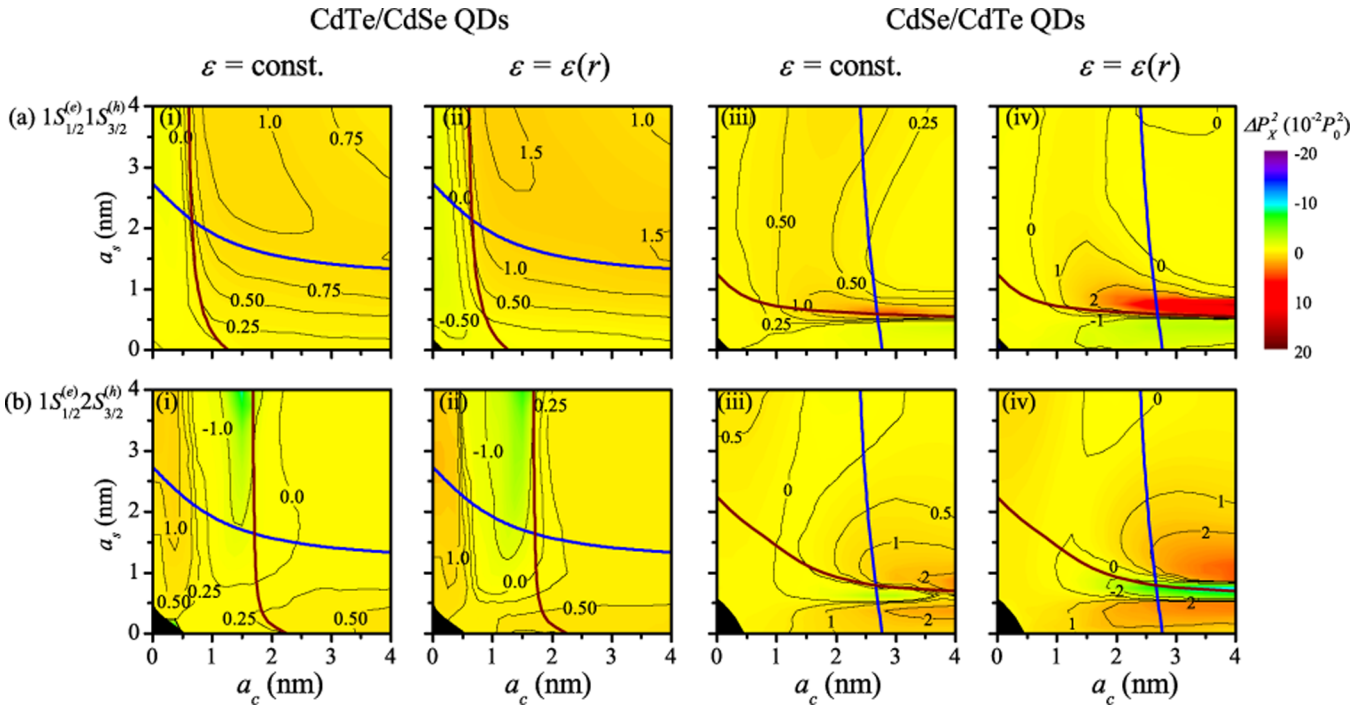

Figure 12. Change ΔP_X^2 in the optical dipole matrix element due to correlation for the (a) $1S^{(e)}_{1/2}1S^{(h)}_{3/2}$ and (b) $1S^{(e)}_{1/2}2S^{(h)}_{3/2}$ excitons in CdTe/CdSe and CdSe/CdTe QDs. (i) and (iii) correspond to ε = const., while (ii) and (iv) correspond to $\varepsilon = \varepsilon(r)$, respectively. Electron (hole) LBs are shown as blue (red) lines.

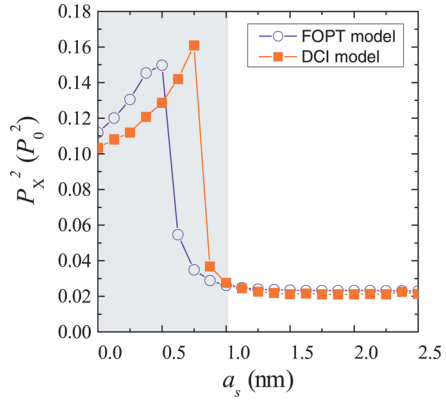

Figure 13. Dipole matrix elements calculated in FOPT (open circles) and the DCI scheme (solid squares) for CdSe/CdTe QDs with a_c = 3.5 nm as a function of the shell thickness for the $1S^{(e)}_{1/2}1S^{(h)}_{3/2}$ exciton. The shaded area shows the region of a_s in which correlation has the greatest effect.

of optoelectronic devices that rely on dynamic processes between charges.

We also found that the effect of correlation on the CdSe/CdTe QD exciton dipoles and radiative lifetimes strongly depends on the dielectric properties of the external medium. In Table 1 we list radiative times calculated with and without correlation for several values of ε_3. The first two rows correspond to the spatially varying dielectric constant $\varepsilon = \varepsilon(r)$ while the third row corresponds to ε = const., i.e., the case without dielectric confinement. Generally, as ε_3 is increased and the dielectric mismatch between the QD and the external medium falls, we see that the effect of correlation on the radiative lifetimes becomes less important. However, for the case of a QD in vacuo or air (ε_3 = 1) and commonly used

Table 1. Radiative Lifetimes of CdSe/CdTe QDs with a_c = 3.5 nm and Different Dielectric Environments[a]

ε_3	a_s (nm)	τ_{rad}^{FOPT} (ns)	τ_{rad}^{DCI} (ns)
1	0.80	38.6	7.66
2	0.75	13.4	2.85
6.65	0.55	1.55	0.96

[a]The second column shows shell widths for which ΔP_X^2 reaches its maximum: τ_{rad}^{FOPT} obtained neglecting the correlation effects and τ_{rad}^{DCI} obtained including them.

solvents like toluene or hexane ($\varepsilon_3 \approx 2$), the effect of correlations on the radiative lifetime cannot be neglected.

Type-II QD heterostructures have smaller dipole matrix elements than core-only QDs of the same ground state exciton energy. Such reduced dipole matrix elements could be beneficial for solar cell applications due to the longer radiative recombination times (and better charge extraction efficiencies) of photoexcited charges compared to core-only QDs.[45]

IV. CONCLUSIONS

We developed a computationally efficient decoupled CI scheme to examine the correlation energy E_{corr} and the change in optical dipole matrix element ΔP_X^2 of the $1S^{(e)}_{1/2}nS^{(h)}_{3/2}$ (n = 1, 2) excitons as a function of core radius and shell width in type-II CdTe/CdSe and CdSe/CdTe core/shell QDs. We have found the following: (i) The QD designs which gave the largest magnitude E_{corr} values for the $1S^{(e)}_{1/2}nS^{(h)}_{3/2}$ (n = 1, 2) excitons were associated with delocalized $ns^{(h)}_{3/2}$ hole states. In CdSe/CdTe QDs the largest magnitude correlation energy found is the consequence of strong configuration mixing of the $1s^{(e)}_{1/2}1s^{(h)}_{3/2}$ and $1s^{(e)}_{1/2}2s^{(h)}_{3/2}$ EHPs in the excitonic wave function caused by dielectric mismatch. (ii) The dielectric confinement mainly affected QDs in the type-I and quasi-type-II localization regimes, particularly those QDs for which the corresponding SP

DOI: 10.1021/acs.jpcc.5b02789
J. Phys. Chem. C 2015, 119, 12720−12730

hole states are delocalized. (iii) Overall CdSe/CdTe QDs were affected more by dielectric environment than CdTe/CdSe QDs, as they tend to localize holes in the shell closer to the repulsive peak in the self-polarization potential that arises from dielectric mismatch. We conclude that the correlated holes are more affected by dielectric confinement than the electrons due to the much larger density of states in the VB. (iv) The regions of (a_c,a_s) space with the largest ΔP_X^2 corresponded to regions in which $|E_{corr}|$ was greatest. The dipole matrix elements of the $1S_{1/2}^{(e)}nS_{3/2}^{(h)}$ (n = 1, 2) excitons can be significantly changed by the dielectric environment in CdSe/CdTe QDs, in contrast to CdTe/CdSe QDs in which they are only slightly affected. These results suggest that changing the dielectric environment could be another way in which to control the oscillator strength and radiative lifetime of excitons in CdSe/CdTe core/shell QDs.

In contrast to epitaxially grown QDs,[45] which largely correspond to the ε = const. case in our analysis, our results show that the charge separation due to the type-II band alignments and by dielectric mismatch induces self-polarization in core/shell colloidal QDs leads to strong deviations from the SCA for the exciton wave function.

APPENDIX

The SP and excitonic states were calculated using the parameters in Table 2, where E_g denotes the bulk band gap,

Table 2. (2,6)-Band k·p Parameters[a]

	CdTe	CdSe	matrix
E_g (eV)	1.56[b]	1.75[b]	8
E_{P_0} (eV)	17.9[c]	17.5[b]	0
Δ (eV)	0.953[c]	0.42[d]	0
E_v (eV)	0 (−0.4)	−0.4 (0)	−3.525 (−3.22)
γ_1^L	5.37[c]	3.33[e]	1
γ_2^L	1.67[c]	1.11[e]	0
γ_3^L	1.98[c]	1.45[e]	0
α	0.965	−1.02	1
m_e^* (m_0)	0.091[c]	0.12[e]	1
ε (ε_0)	7.1[f]	6.2[g]	2

[a]E_v values correspond to the CdTe/CdSe (CdSe/CdTe) VB offsets. [b]Reference 46. [c]Reference 37. [d]Reference 47. [e]Reference 48. [f]Reference 49. [g]Reference 50.

the Kane energy is $E_{P_0} = 2m_0P_0^2/\hbar^2$, P_0 is the bulk interband momentum matrix element, m_0 is the free electron mass,[41] Δ is the spin−orbit splitting, and E_v is the VBM energy. The Luttinger parameters are γ_i^L (i = 1, 2, 3), α is a CB parameter, and m_e^* represents the electron effective mass at the bottom of the CB;[37] ε is the dielectric constant given in the units of free space permitivity, ε_0. Modified Luttinger parameters for the VB were calculated in the spherical approximation.[36]

AUTHOR INFORMATION

Corresponding Author

*E-mail: s.tomic@salford.ac.uk. Tel.: +44(0)1612-953847.

Notes

The authors declare no competing financial interest.

ACKNOWLEDGMENTS

The authors acknowledge the EPSRC U.K. grant "Enhanced multiple exciton generation in colloidal quantum dots" (EP/K008587/1) for financial support. We also acknowledge the EU-COST project "MultiscaleSolar" (MP1406) and The Great Britain Sasakawa Foundation. We wish to thank Jason Smith and David Binks for useful discussions.

REFERENCES

(1) Pal, B. N.; Ghosh, Y.; Brovelli, S.; Laocharoensuk, R.; Klimov, V. I.; Hollingsworth, J. A.; Htoon, H. Giant CdSe/CdS Core/Shell nanocrystal quantum dots as efficient electroluminescent materials: strong influence of shell thickness on light-emitting diode performance. *Nano Lett.* **2012**, *12*, 331−336.

(2) Kamat, P. V. Quantum dot solar cells: semiconductor nanocrystals as light harvesters. *J. Phys. Chem. C* **2008**, *112*, 18737−18753.

(3) Sukhovatkin, V.; Hinds, S.; Brzozowski, L.; Sargent, E. H. Colloidal Quantum-dot photodetectors exploiting multiexciton generation. *Science* **2009**, *324*, 1542−1544.

(4) Konstantatos, G.; Sargent, E. H. Nanostructured materials for photon detection. *Nat. Nanotechnol.* **2010**, *5*, 391−400.

(5) Caruge, J.-M.; Chan, Y.; Sundar, V.; Eisler, H. J.; Bawendi, M. G. Transient photoluminescence and simultaneous amplified spontaneous emission from multiexciton states in CdSe quantum dots. *Phys. Rev. B* **2004**, *70*, 085316.

(6) Klimov, V. I.; Ivanov, S. A.; Nanda, J.; Achermannn, M.; Bezel, I.; McGuire, J. A.; Piryatinski, A. Single-exciton optical gain in semiconductor nanocrystals. *Nature* **2007**, *447*, 441−446.

(7) Shabaev, A.; Efros, A. L.; Nozik, A. J. Multiexciton generation by a single photon in nanocrystals. *Nano Lett.* **2006**, *6*, 2856−2863.

(8) Semonin, O. E.; Luther, J. M.; Choi, S.; Chen, H.-Y.; Gao, J.; Nozik, A. J.; Beard, M. C. Peak external photocurrent quantum efficiency exceeding 100% via MEG in a quantum dot solar cell. *Science* **2011**, *334*, 1530−1533.

(9) Trinh, M. T.; Polak, L.; Schins, J. M.; Houtepen, A. J.; Vaxenburg, R.; Maikov, G. I.; Grinbom, G.; Midgett, A. G.; Luther, J. M.; Beard, M. C.; Nozik, A. J.; Bonn, M.; Lifshitz, E.; Siebbeles, L. D. A. Anomalous independence of multiple exciton generation on different group IV-VI quantum dot architectures. *Nano Lett.* **2011**, *11*, 1623−1629.

(10) Ithurria, S.; Tessier, M. D.; Mahler, B.; Lobo, R. P. S. M.; Dubertret, B.; Efros, A. L. Colloidal nanoplatelets with two-dimensional electronic structure. *Nat. Mater.* **2011**, *10*, 936−941.

(11) Jasieniak, J.; Califano, M.; Watkins, S. E. Size-dependent valence and conduction band-edge energies of semiconductor nanocrystals. *ACS Nano* **2011**, *5*, 5888−5902.

(12) Kim, S.; Fisher, B.; Eisler, H.-J.; Bawendi, M. Type-II quantum dots: CdTe/CdSe(core/shell) and CdSe/ZnTe(core/shell) heterostructures. *J. Am. Chem. Soc.* **2003**, *125*, 11466−11467.

(13) Li, J. J.; Tsay, J. M.; Michalet, X.; Weiss, S. Wavefunction engineering: from quantum wells to near-infrared type-II colloidal quantum dots synthesized by layer-by-layer colloidal epitaxy. *Chem. Phys.* **2005**, *318*, 82−90.

(14) Xie, R.; Kolb, U.; Li, J.; Basché, T.; Mews, A. Synthesis and characterization of highly luminescent CdSe-Core $CdS/Zn_{0.5}Cd_{0.5}$ S/ZnS multishell nanocrystals. *J. Am. Chem. Soc.* **2005**, *127*, 7480−7488.

(15) Piryatinski, A.; Ivanov, S. A.; Tretiak, S.; Klimov, V. I. Effect of quantum and dielectric confinement on the exciton-exciton interaction energy in type II core/shell semiconductor nanocrystals. *Nano Lett.* **2007**, *7*, 108−115.

(16) Kumar, S.; Jones, M.; Lo, S.; Scholes, G. D. Nanorod heterostructures showing photoinduced charge separation. *Small* **2007**, *3*, 1633−1639.

(17) Zhong, H.; Zhou, Y.; Yang, Y.; Yang, C.; Li, Y. Synthesis of type II CdTe-CdSe nanocrystal heterostructured multiple-branched rods and their photovoltaic applications. *J. Phys. Chem. C* **2007**, *111*, 6538−6543.

(18) Itzhakov, S.; Shen, H.; Buhbut, S.; Lin, H.; Oron, D. Type-II quantum-dot-sensitized solar cell spanning the visible and near-infrared spectrum. *J. Phys. Chem. C* **2013**, *117*, 22203−22210.

DOI: 10.1021/acs.jpcc.5b02789
J. Phys. Chem. C 2015, 119, 12720−12730

(19) McElroy, N.; Page, R.; Espinbarro-Valazquez, D.; Lewis, E.; Haigh, S.; O'Brien, P.; Binks, D. Comparison of solar cells sensitised by CdTe/CdSe and CdSe/CdTe core/shell colloidal quantum dots with and without a CdS outer layer. *Thin Solid Films* **2014**, *560*, 65−70.
(20) Brovelli, S.; Schaller, R. D.; Crooker, S. A.; Garcia-Santamaria, F.; Chen, Y.; Viswanatha, R.; Hollingsworth, J. A.; Htoon, H.; Klimov, V. I. Nano-engineered electron-hole exchange interaction controls exciton dynamics in core-shell semiconductor nanocrystals. *Nat. Commun.* **2011**, *2*, 280.
(21) Oron, D.; Kazes, M.; Banin, U. Multiexcitons in type-II colloidal semiconductor quantum dots. *Phys. Rev. B* **2007**, *75*, 035330.
(22) McDonald, P. G.; Tyrrell, E. J.; Shumway, J.; Smith, J. M.; Galbraith, I. Tuning biexciton binding and antibinding in core/shell quantum dots. *Phys. Rev. B* **2012**, *86*, 125310.
(23) Ivanov, S. A.; Nanda, J.; Piryatinski, A.; Achermann, M.; Balet, L. P.; Bezel, I. V.; Anikeeva, P. O.; Tretiak, S.; Klimov, V. I. Light amplification using inverted core/shell nanocrystals: towards lasing in the single-exciton regime. *J. Phys. Chem. B* **2004**, *108*, 10625−10630.
(24) Nanda, J.; Ivanov, S. A.; Achermann, M.; Bezel, I.; Piryatinski, A.; Klimov, V. I. Light amplification in the single-exciton regime using exciton-exciton repulsion in type-II nanocrystal quantum dots. *J. Phys. Chem. C* **2007**, *111*, 15382−15390.
(25) Szabo, A.; Ostlund, N. S. *Modern Quantum Chemistry: Introduction to Advanced Electronic Structure Theory*; Dover Publications, Inc.: Mineola, NY, 1982.
(26) Fonoberov, V. A.; Pokatilov, E. P.; Balandin, A. A. Exciton states and optical transitions in colloidal CdS quantum dots: Shape and dielectric mismatch effects. *Phys. Rev. B* **2002**, *66*, 085310.
(27) Menéndez-Proupin, E.; Trallero-Giner, C. Electric-field and exciton structure in CdSe nanocrystals. *Phys. Rev. B* **2004**, *69*, 125336.
(28) Vukmirovć, N.; Tomić, S. Plane wave methodology for single quantum dot electronic structure calculations. *J. Appl. Phys.* **2008**, *103*, 103718.
(29) Califano, M.; Franceschetti, A.; Zunger, A. Lifetime and polarization of the radiative decay of excitons, biexcitons, and trions in CdSe nanocrystal quantum dots. *Phys. Rev. B* **2007**, *75*, 115401.
(30) Korkusinski, M.; Voznyy, O.; Hawrylak, P. Fine structure and size dependence of exciton and biexciton optical spectra in CdSe nanocrystals. *Phys. Rev. B* **2010**, *82*, 245304.
(31) Allan, G.; Delerue, C. Tight-binding calculations of the optical properties of HgTe nanocrystals. *Phys. Rev. B* **2012**, *86*, 165437.
(32) Efros, A. L.; Rosen, M. The electronic structure of semiconductor nanocrystals. *Annu. Rev. Mater. Sci.* **2000**, *30*, 475−521.
(33) Franceschetti, A.; Williamson, A.; Zunger, A. Addition spectra of quantum dots: the role of dielectric mismatch. *J. Phys. Chem. B* **2000**, *104*, 3398−3401.
(34) Climente, J. I.; Royo, M.; Movilla, J. L.; Planelles, J. Strong configuration mixing due to dielectric confinement in semiconductor nanorods. *Phys. Rev. B* **2009**, *79*, 161301.
(35) Brus, L. E. Electron-electron and electron-hole interactions in small semiconductor crystallites: The size dependence of the lowest excited electronic state. *J. Chem. Phys.* **1984**, *80*, 4403−4409.
(36) Pokatilov, E. P.; Fonoberov, V. A.; Fomin, V. M.; Devreese, J. T. Development of an eight-band theory for quantum dot heterostructures. *Phys. Rev. B* **2001**, *64*, 245328.
(37) Efros, A. L.; Rosen, M. Quantum size level structure of narrow-gap semiconductor nanocrystals: effect of band coupling. *Phys. Rev. B* **1998**, *58*, 7120−7135.
(38) Bolcatto, P. G.; Proetto, C. R. Partially confined excitons in semiconductor nanocrystals with a finite size dielectric interface. *J. Phys.: Condens. Matter* **2001**, *13*, 319.
(39) Tyrrell, E. J.; Smith, J. M. Effective mass modeling of excitons in type-II quantum dot heterostructures. *Phys. Rev. B* **2011**, *84*, 165328.
(40) Brus, L. E. A simple model for the ionization potential, electron affinity, and aqueous redox potentials of small semiconductor crystallites. *J. Chem. Phys.* **1983**, *79*, 5566−5571.
(41) Efros, A. L.; Rosen, M.; Kuno, M.; Nirmal, M.; Norris, D. J.; Bawendi, M. Band-edge exciton in quantum dots of semiconductors with a degenerate valence band: Dark and bright exciton states. *Phys. Rev. B* **1996**, *54*, 4843−4856.
(42) Gong, K.; Zeng, Y.; Kelley, D. F. Extinction coefficients, oscillator strengths, and radiative lifetimes of CdSe, CdTe, and CdTe/CdSe nanocrystals. *J. Phys. Chem. C* **2013**, *117*, 20268−20279.
(43) Ma, X.; Mews, A.; Kipp, T. Determination of electronic energy levels in type-II CdTe-core/CdSe-shell and CdSe-core/CdTe-shell nanocrystals by cyclic voltammetry and optical spectroscopy. *J. Phys. Chem. C* **2013**, *117*, 16698−16708.
(44) Cai, X.; Mirafzal, H.; Nguyen, K.; Leppert, V.; Kelley, D. F. Spectroscopy of CdTe/CdSe type-II nanostructures: morphology, lattice mismatch, and band-bowing effects. *J. Phys. Chem. C* **2012**, *116*, 8118−8127.
(45) Tomić, S. Effect of Sb induced type II alignment on dynamical processes in InAs/GaAs/GaAsSb quantum dots: Implication to solar cell design. *Appl. Phys. Lett.* **2013**, *103*, 072112.
(46) de Mello Donegá, C.; Koole, R. Size dependence of the spontaneous emission rate and absorption cross section of CdSe and CdTe quantum dots. *J. Phys. Chem. C* **2009**, *113*, 6511−6520.
(47) Norris, D. J.; Bawendi, M. G. Measurement and assignment of the size-dependent optical spectrum in CdSe quantum dots. *Phys. Rev. B* **1996**, *53*, 16338−16346.
(48) Schulz, S.; Czycholl, G. Tight-binding model for semiconductor nanostructures. *Phys. Rev. B* **2005**, *72*, 165317.
(49) Rowe, J. M.; Nicklow, R. M.; Price, D. L.; Zanio, K. Lattice dynamics of cadmium telluride. *Phys. Rev. B* **1974**, *10*, 671−675.
(50) Wang, L.-W.; Zunger, A. Pseudopotential calculations of nanoscale CdSe quantum dots. *Phys. Rev. B* **1996**, *53*, 9579−9582.
(51) The factor of 1/4 comes from the Clebsch−Gordan coefficient in eq 5 when $L = L_z = 1$, $j_e = 1/2$, $m_e = 1/2$, $j_h = 3/2$, and $m_h = 1$.
(52) Additional calculations for the $1S^{(e)}_{1/2}nS^{(h)}_{3/2}$ ($n = 1, 2$) states show that the relative error between exciton energies is a function of a_c and a_s, but does not exceed 1%.

DOI: 10.1021/acs.jpcc.5b02789
J. Phys. Chem. C 2015, 119, 12720−12730